

Localization of Anatomical Point Landmarks in 3D Medical Images by Fitting 3D Parametric Intensity Models

Stefan Wörz and Karl Rohr

School of Information Technology, Computer Vision & Graphics Group
International University in Germany, 76646 Bruchsal
Email: {woerz,rohr}@i-u.de

Abstract. We introduce a new approach for the localization of 3D anatomical point landmarks. The approach uses 3D parametric intensity models of anatomical structures which are directly fit to the image intensities. We developed an analytic model based on the Gaussian error function to efficiently model tip-like structures of ellipsoidal shape. The approach has been successfully applied to accurately localize the tips of ventricular horns in 3D MR image data.

1 Introduction

The localization of 3D anatomical point landmarks is an important task in medical image analysis. Landmarks are useful image features in a variety of applications, for example, the registration of 3D brain images of different modalities or the registration of images with digital atlases. The current standard procedure, however, is to localize 3D anatomical point landmarks manually which is difficult, time consuming, and error-prone. To improve the current situation it is therefore important to develop automated methods.

In previous work on the localization of anatomical point landmarks, 3D differential operators have been proposed (e.g., Thirion [1], Rohr [2]). For a recent evaluation study of nine different 3D differential operators see Hartkens *et al.* [3]. While being computationally efficient, differential operators incorporate only small local neighbourhoods of an image and are therefore relatively sensitive to noise, which leads to false detections and also affects the localization accuracy. Recently, an approach based on deformable models was introduced, see Frantz *et al.* [4] and Alker *et al.* [5]. With this approach tip-like anatomical structures are modeled by surface models, which are fit to the image data using an edge-based fitting measure. However, the approach requires the detection of 3D image edges as well as the formulation of a relatively complicated fitting measure, which involves the image gradient as well as 1st order derivatives of the surface model.

We have developed a new approach for the localization of 3D anatomical point landmarks. In contrast to previous approaches the central idea is to use 3D parametric intensity models of anatomical structures. In comparison to differential approaches, larger image regions and thus semi-global image information

is taken into account. In comparison to approaches based on surface models, we directly exploit the intensity information of anatomical structures. Therefore, more a priori knowledge and much more image information is taken into account in our approach to improve the robustness against noise and to increase the localization accuracy.

2 Parametric Intensity Model for Tip-Like Structures

Our approach uses 3D parametric intensity models which are fit directly to the intensities of the image data (see Rohr [6] where such an approach has been proposed for segmenting 2D corner and edge features). These models describe the image intensities of anatomical structures in a semi-global region as a function of a certain number of parameters. The main characteristic, e.g. in comparison to general deformable models, is that they exhibit a prominent point which defines the position of the landmark. By fitting the parametric intensity model to the image intensities we obtain a subvoxel estimate of the position as well as estimates of the other parameters, e.g., the image contrast. As an important class of 3D anatomical point landmarks we here consider tip-like structures. Such structures can be found, for example, within the human head at the ventricular system (e.g., the tips of the frontal, occipital, or temporal horns) and at the skull (e.g., the tip of the external occipital protuberance).

The shape of these anatomical structures is ellipsoidal. Therefore, we use a (half-)ellipsoid with the three semi-axes (r_x, r_y, r_z) and the intensity levels a_0 (outside) and a_1 (inside) to model them. We also introduce Gaussian smoothing with the parameter σ to incorporate image smoothing effects. To efficiently represent the resulting 3D intensity structure we developed an analytic model based on $\Phi(x) = \int_{-\infty}^x (2\pi)^{-1/2} e^{-\xi^2/2} d\xi$, which is given by

$$g_{Ell.}(\mathbf{x}) = a_0 + (a_1 - a_0) \Phi \left(\frac{\sqrt[3]{r_x r_y r_z}}{\sigma} \left(1 - \sqrt{\frac{x^2}{r_x^2} + \frac{y^2}{r_y^2} + \frac{(z + r_z)^2}{r_z^2}} \right) \right) \quad (1)$$

where $\mathbf{x} = (x, y, z)$. We define the tip of the ellipsoid w.r.t. the semi-axis r_z as the position of the landmark, which also is the center of the local coordinate system. In addition, we include a 3D rigid transform \mathcal{R} with translation parameters (x_0, y_0, z_0) and rotation parameters (α, β, γ) . Moreover, we extend our model to a more general class of tip-like structures by applying a tapering deformation \mathcal{T} with the parameters ρ_x and ρ_y , and a bending deformation \mathcal{B} with the parameters δ (strength) and ν (direction), which are defined by

$$\mathcal{T}(\mathbf{x}) = \begin{pmatrix} x(1 + z\rho_x/r_z) \\ y(1 + z\rho_y/r_z) \\ z \end{pmatrix} \quad \text{and} \quad \mathcal{B}(\mathbf{x}) = \begin{pmatrix} x - z^2\delta\cos\nu \\ y - z^2\delta\sin\nu \\ z \end{pmatrix} \quad (2)$$

This results in our parametric intensity model with a total of 16 parameters:

$$g_M(\mathbf{x}, \mathbf{p}) = g_{Ell.}(\mathcal{T}(\mathcal{B}(\mathcal{R}(\mathbf{x})))) \quad (3)$$

$$\mathbf{p} = (r_x, r_y, r_z, a_0, a_1, \sigma, \rho_x, \rho_y, \delta, \nu, \alpha, \beta, \gamma, x_0, y_0, z_0) \quad (4)$$

3 Model Fitting Approach

Estimates for the model parameters are found by a least-squares fit of the model to the image intensities $g(\mathbf{x})$ within semi-global regions-of-interest (ROIs), thus minimizing

$$\sum_{\mathbf{x} \in \text{ROI}} (g_M(\mathbf{x}, \mathbf{p}) - g(\mathbf{x}))^2 \quad (5)$$

The fitting measure does not include any derivatives. This is in contrast to previous fitting measures for surface models which incorporate the image gradient as well as 1st order derivatives of the model (e.g., [4]). For the minimization we apply the method of Levenberg-Marquardt, incorporating 1st order partial derivatives of the intensity model w.r.t. the model parameters, which can be derived analytically. Note, we do not need the image gradient. We need 1st order derivatives of the intensity model only for the minimization process, whereas the surface model approach requires 2nd order derivatives for the minimization.

To improve the robustness as well as the accuracy of model fitting, we separated the model fitting process into different phases. In the first phase, only a subset of the model parameters are allowed to vary in the minimization process (parameters for semi-axes, rotation, and smoothing). In subsequent phases further model parameters are additionally allowed to vary, i.e. the parameters of the translation, the intensity levels, and the deformation.

4 Experimental Results

Our approach has been applied to 3D synthetic data as well as to 3D MR images of the human head. In the first part of the synthetic experiments, we applied our approach to 3D image data generated by the model itself with added Gaussian noise. In total we carried out about 2400 experiments and achieved a very high localization accuracy with an error in the estimated position of less than 0.12 voxels. We also found that the approach is robust w.r.t. the choice of initial parameters. In the second part, we applied our approach to synthetic 3D images, which have been obtained by discrete Gaussian smoothing of an ideal (unsmoothed) ellipsoid. Since our 3D model represents an approximation to a

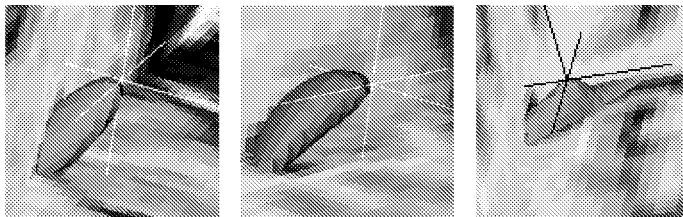


Fig. 1. 3D contour plots of the fitted model for the left temporal horn (left), the right temporal horn (center), and the right occipital horn (right) within the original data. The marked axes indicate the estimated landmark positions.

Gaussian smoothed ellipsoid, in these experiments it turned out that we obtained a systematic error in estimating the landmark position. To cope with these errors we developed a nonlinear correction function which “calibrates” the model: $\Delta z_0 = c_1 + c_2\hat{\sigma} + c_3\hat{\sigma}^2 + (c_4 + c_5\hat{\sigma} + c_6\hat{\sigma}^2) 2\hat{r}_z / (\hat{r}_x + \hat{r}_y)$. To determine the parameters c_1, \dots, c_6 we devised a large number of experiments and systematically varied the respective parameters. In total, we used more than 2000 synthetic 3D images. Incorporating the correction function, we achieved an average localization error of less than 0.2 voxels.

We also applied our approach to real 3D MR images of the human head. Table 1 shows the fitting results for the tips of six ventricular horns. For each landmark, we applied the model fitting 100 times with different sets of initial parameters. On average, model fitting succeeded in 89 cases with an average of 75 iterations and a mean fitting error (positive root of the mean squared error) of $\bar{e}_{int} = 10.70$. The average distance between the estimated landmark positions and manually localized positions for all six landmarks is $\bar{e} = 1.90$ voxels. In comparison, using the 3D differential operator Op3 ([2]), we obtain an average distance of $\bar{e}_{Op3} = 3.42$ voxels. Thus, the localization accuracy with our new approach turns out to be much better. For three landmarks we have also visualized the fitting results in Figure 1 using 3D Slicer (SPL, Boston). It demonstrates that the spectrum of possible shapes of our model is relatively large. The left ellipsoid includes only tapering, the center ellipsoid includes tapering and bending, and the right ellipsoid includes relatively strong tapering and bending. Figure 2 shows the fitting results for the left and right frontal horn overlaid with four different slices of the original data. It can be seen that the model describes the depicted anatomical structures fairly well.

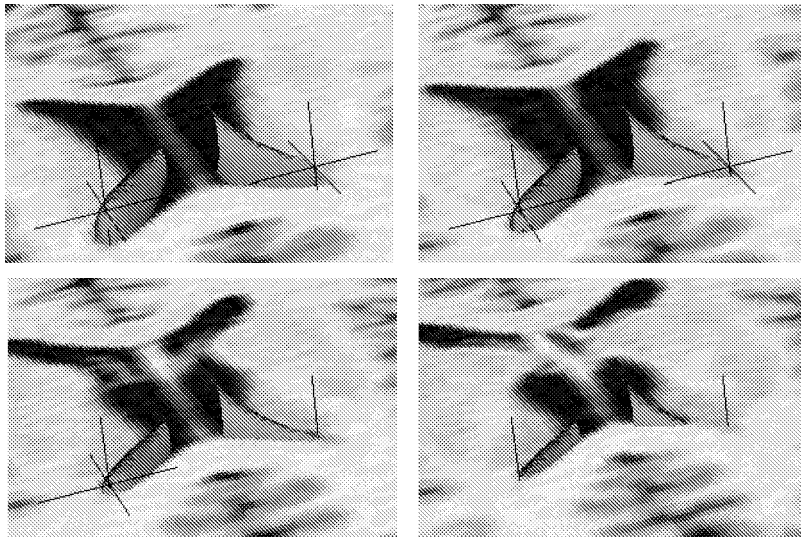


Fig. 2. 3D contour plots of the fitted model for the left and right frontal horn. The result is shown for four different slices of the original data.

Table 1. Fitting results for the ventricular horns in a 3D MR image for ca. 100 experiments using a spherical ROI with a diameter of 21 (*11) voxels. The estimated landmark position and intensity levels are given with their standard deviations. Also, the mean fitting error \bar{e}_{int} and the distance \bar{e} to the manually localized landmark position are listed. For comparison, the distance \bar{e}_{Op3} of the diff. operator $Op3$ is given.

Landmark	\hat{x}_0	\hat{y}_0	\hat{z}_0	\hat{a}_0	\hat{a}_1	\bar{e}_{int}	\bar{e}	\bar{e}_{Op3}
Left frontal horn	111.17	78.36	101.79	124.7	23.1	9.13	2.20	3.16
(Tapering only)	0.001	0.001	0.001	0.01	0.01			
Right frontal horn	111.48	76.64	132.80	122.7	19.4	10.69	2.32	2.24
(Tapering only)	0.002	0.001	0.002	0.01	0.03			
Left occipital horn	189.38	101.53	91.58	107.3	23.4	10.17	2.30	4.12
(Tapering and bending)*	0.089	0.078	0.204	0.13	0.24			
Right occipital horn	182.61	97.22	150.01	112.7	19.4	7.81	0.87	3.61
(Tapering and bending)*	0.063	0.025	0.109	0.07	3.53			
Left temporal horn	134.63	111.65	90.05	106.7	43.0	13.36	2.81	2.83
(Tapering only)	0.031	0.023	0.014	0.01	0.21			
Right temporal horn	130.36	114.79	148.92	104.9	26.3	13.03	0.87	4.58
(Tapering and bending)	0.008	0.030	0.026	0.01	0.11			

5 Discussion

The experiments verify the applicability of our new approach, which yields sub-voxel positions of 3D anatomical landmarks. In further work we plan to perform a comprehensive evaluation study including a comparison with the results of other approaches.

6 Acknowledgement

The 3D MR image data has been kindly provided by Philips Research Laboratories Hamburg.

References

1. J.-P. Thirion, "New Feature Points based on Geometric Invariants for 3D Image Registration", *Int. J. of Computer Vision* 18:2, 1996, 121-137
2. K. Rohr, "On 3D differential operators for detecting point landmarks", *Image and Vision Computing* 15:3, 1997, 219-233
3. T. Hartkens, K.Rohr, H.S. Stiehl, "Evaluation of 3D Operators for the Detection of Anatomical Point Landmarks in MR and CT Images", *CVIU* 85, 2002, 1-19
4. S. Frantz, K. Rohr, and H.S. Stiehl, "Localization Of 3D Anatomical Point Landmarks In 3D Tomographic Images Using Deformable Models", *Proc. MICCAI 2000*, Springer, 2000, 492-501
5. M. Alker, S. Frantz, K. Rohr, and H.S. Stiehl, "Hybrid Optimization for 3D Landmark Extraction: Genetic Algorithms and Conjugate Gradient Method", *Proc. BVM 2002*, Springer, 2002, 314-317
6. K. Rohr, "Recognizing Corners by Fitting Parametric Models", *International J. of Computer Vision* 9:3, 1992, 213-230